FREQUENCY DOMAIN TURBO EQUALIZATION FOR VESTIGIAL SIDEBAND MODULATION WITH PUNCTURED TRELLIS CODING

Hong Liu, Philip Schniter

The Ohio State University
Dept. of ECE
2015 Neil Avenue, Columbus, OH 43210

Haosong Fu, Raúl A. Casas

ATI Research, Inc.
770 Township Line Road Suite 200
Yardley, PA 19067

ABSTRACT

This work proposes a frequency domain turbo equalization (FDTE) scheme for the reception of transmissions that employ vestigial sideband modulation and punctured trellis coding, as specified by the ATSC North American terrestrial digital television (DTV) standard. The proposed FDTE scheme enables low-cost and high performance reception of highly impaired DTV signals. Through numerical simulation, we demonstrate that our FDTE scheme outperforms the traditional joint DFE/decoding approach at a fraction of the implementation cost.

1. INTRODUCTION

The performance of ATSC [1] digital television (DTV) receivers has been steadily increasing over the last decade [2, 3]. Receivers have become increasingly reliable in difficult channel conditions, such as indoor reception in urban settings, where dense multipath can heavily impair the transmitted signal. The current state-of-the-art ATSC reception scheme employs decision feedback equalization (DFE) [4,5]. To handle difficult channels, receiver complexity—in particular, the DFE filter length—has increased significantly. While first-generation ATSC receivers typically employed DFEs with 100 forward and 400 feedback taps, current-generation receivers typically employ DFEs with 500 forward and 600 feedback taps. If broadcasters adopt the use of repeaters and distributed transmitters to increase coverage [6], then further increases in filter lengths can be expected.

This work proposes a new ATSC receiver architecture based on frequency domain turbo equalization (FDTE). Turbo equalization [7, 8] is an iterative reception scheme whereby the equalizer and decoder iteratively exchange soft information as a computationally efficient means of jointly exploiting channel structure and code structure. While the first turbo-equalization schemes employed *maximum a posteriori* (MAP) equalization [7], it has been suggested more recently to employ linear equalization for complexity reduction [8]. For channels with large delay spreads, which commonly encountered in DTV applications, even linear equalization can be quite costly when implemented in the time domain, as suggested by DFE filter lengths mentioned earlier. For such channels, it might be more effective to consider frequency-domain equalization (FDE), which leverages fast circular convolution via the FFT to drastically reduce the cost of implementing long filters [9]. With non-CP single-carrier transmissions, FDE is complicated by the need for both inter-block interference (IBI) cancellation and CP reconstruction, though these can be performed iteratively [10]. For DTV applications, FDTE is further complicated by the ATSC's use of 8-ary vestigial sideband modulation (8-VSB) and punctured trellis coding. Thus, we propose a novel FDTE scheme suitable for non-CP 8-VSB modulation and punctured trellis coding. Through numerical comparisons, we find that the proposed scheme gives simultaneous performance and complexity gains over time-domain DFE reception.

The paper is organized as follows. Section 2 briefly describes the communication system model. Section 3 details the multiple stages of our FDTE algorithm, including cyclic-prefix restoration (CPR), minimum mean square error equalization (MMSE), update of priori information, and block overlapping. Section 4 compares our FDTE to time-domain DFE using a channel model that is commonly employed for DTV receiver evaluation.

In this paper, we use upper (lower) bold face notation for matrices (column vectors), $\boldsymbol{I}_p$ for the $p \times p$ identity matrix, $\mathbf{0}_{M\times N}$ for the $M \times N$ zero matrix, and $\mathbf{1}_N$ for the $N \times 1$ vector of ones. We use $\mathcal{D}(\boldsymbol{a})$ for the diagonal matrix with $\boldsymbol{a}$ as its diagonal, and $\mathrm{diag}(\cdot)$ to denote the extraction of the main diagonal of a matrix. Finally, we use $\boldsymbol{A}^*$, $\boldsymbol{A}^T$, and $\boldsymbol{A}^H$ to denote the conjugate, transpose, and Hermitian transpose of $\boldsymbol{A}$, respectively.

2. SYSTEM MODEL

Consider a VSB modulated system where a stream of real-valued finite-alphabet symbols $\{s_n\}$ is transmitted over a noisy linear time-varying (LTV) multipath channel. The channel, including the effect of VSB pulse shaping, can be described by the order-L complex-valued impulse response $\{h_{n,l}\}_{l=0}^{L}$, where $h_{n,l}$ denotes the time-n response to an impulse applied at time $n-l$. Such a system yields the complex-valued observations $\{r_n\}$,

$$r_n \;=\; \sum_{l=0}^{L} h_{n,l}\, s_{n-l} + \nu_n. \tag{1}$$

where $\{\nu_n\}$ is assumed to be circular white Gaussian noise (CWGN) with mean zero and variance σ^2. Since two real-valued observations are made for every real-valued symbol s_n, one might consider (1) to be oversampled by a factor of two.

For our FDTE scheme, we assume block-wise processing with block length N. In fact, we focus on overlapping blocks, with block interval $N_D < N$. Furthermore, we assume that the channel is time-invariant over the duration of a single block. For convenience, we define the block-based quantities $r_n(i) = r_{iN_D+n}$, $h_l(i) = h_{iN_D,l}$, $s_n(i) = s_{iN_D+n}$, and $\nu_n(i) = \nu_{iN_D+n}$, and their vector counterparts $\boldsymbol{r}(i) := [r_0(i), r_1(i), \ldots, r_{N-1}(i)]$, $\boldsymbol{s}(i) :=$

This work supported in part by the ATI DTV Group in Yardley, PA.

$[s_0(i), s_1(i), \ldots, s_{N-1}(i)]$, $\boldsymbol{h}(i) := [h_0(i), h_1(i), \ldots, h_{N-1}(i)]$, and $\boldsymbol{\nu}(i) := [\nu_0(i), \nu_1(i), \ldots, \nu_{N-1}(i)]$. Thus, the signal received during the i-th block can be expressed as

$$r_n(i) = \begin{cases} \nu_n^{(i)} + \sum_{l=0}^{n} h_l(i) s_{n-l}(i) \\ \quad + \sum_{l=n+1}^{L} h_l(i) s_{<n-l>_N}(i-1) & , \quad 0 \le n < L, \\ \nu_n^{(i)} + \sum_{l=0}^{L} h_l(i) s_{n-l}(i), & L \le n < N, \end{cases} \tag{2}$$

where $< n >_N$ denotes n modulo N. Note that the samples $\{r_n(i)\}_{n=0}^{L-1}$ contain inter-block interference (IBI) from $\boldsymbol{s}(i-1)$.

3. FREQUENCY DOMAIN TURBO EQUALIZATION

Figure 1 illustrates the steps involved for FDTE reception. At each iteration m, the FDTE performs the following steps:

1. Perform IBI cancellation and CP reconstruction on $\boldsymbol{r}(i)$ to obtain $\boldsymbol{r}_{\text{cpr}}^{(m)}(i)$.
2. Transform the CP-restored time-domain observation $\boldsymbol{r}_{\text{cpr}}^{(m)}(i)$ to the frequency domain observation $\boldsymbol{x}^{(m)}(i)$ via FFT.
3. Calculate MMSE-based virtual subcarrier estimates $\hat{\boldsymbol{t}}^{(m)}(i)$ assuming prior means $\bar{\boldsymbol{t}}^{(m-1)}(i)$ and variances $\boldsymbol{v}_t^{(m-1)}(i)$.
4. Transform the virtual subcarrier estimates $\hat{\boldsymbol{t}}^{(m)}(i)$ to the time-domain symbol estimates $\hat{\boldsymbol{s}}^{(m)}(i)$ via inverse FFT.
5. Generate conditional probabilities from $\hat{\boldsymbol{s}}^{(m)}(i)$ and use as priors for MAP decoding.
6. Perform MAP decoding.
7. Update the virtual-subcarrier statistics $\bar{\boldsymbol{t}}^{(m)}(i)$, $\boldsymbol{v}_t^{(m)}(i)$, and $\bar{\boldsymbol{s}}^{(m)}(i)$ using the MAP decoder outputs.

We now describe several of these steps in detail.

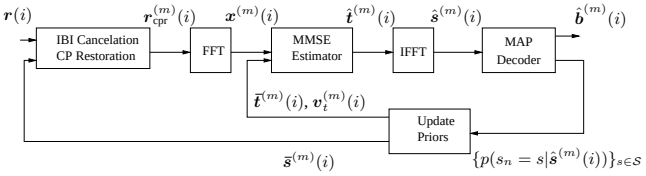

Fig. 1. The proposed frequency domain turbo equalizer.

3.1. IBI Cancellation and CP Restoration

As in [11], we perform IBI cancellation with $\{\hat{s}_n(i-1)\}$, the final estimates of previous-block symbols, and CP reconstruction with $\{\bar{s}_n^{(m-1)}(i)\}$, the most recent estimates of current-block symbols.

$$r_{\text{cpr},n}^{(m)}(i) = \begin{cases} r_n(i) - \sum_{l=n+1}^{L} h_l(i) \hat{s}_{<n-l>_N}(i-1) \\ \quad + \sum_{l=n+1}^{L} h_l(i) \bar{s}_{<n-l>_N}^{(m-1)}(i) & , \quad 0 \le n < L, \\ r_n(i) & L \le n < N. \end{cases} \tag{3}$$

When $m = 1$, $\bar{\boldsymbol{s}}^{(m-1)}(i)$ is replaced by a linear estimate of $\boldsymbol{s}(i)$ obtained from $\boldsymbol{r}(i+1)$ and $\boldsymbol{r}(i)$ as specified in [13].

3.2. MMSE Estimation of Virtual Subcarriers

We assume that CP restoration has been perfectly executed, so that $\boldsymbol{r}_{\text{cpr}}^{(m)}(i)$ can be considered as a noise-corrupted output of a circular convolution between the channel $\boldsymbol{h}(i)$ and the transmitted symbols $\boldsymbol{s}(i)$. For notational brevity, the symbol index (i) and iteration index $^{(m)}$ will be suppressed for the remainder of this section. Assuming perfect CPR, the time-domain system model can be rewritten in matrix form as

$$\boldsymbol{r}_{\text{cpr}} \;=\; \mathcal{C}(\boldsymbol{h})\boldsymbol{s} + \boldsymbol{\nu}, \tag{4}$$

where $\mathcal{C}(\boldsymbol{h})$ denotes the circulant matrix with first column $\boldsymbol{h}$. Taking the discrete Fourier transform (DFT) of (4), we obtain

$$\boldsymbol{x} \;=\; \mathcal{D}(\boldsymbol{g})\boldsymbol{t} + \boldsymbol{w}, \tag{5}$$

where $\boldsymbol{x}$, $\boldsymbol{g}$, $\boldsymbol{t}$ and $\boldsymbol{w}$ denote DFTs of $\boldsymbol{r}_{\text{cpr}}$, $\boldsymbol{h}$, $\boldsymbol{s}$ and $\boldsymbol{\nu}$, respectively. We refer to the elements in $\boldsymbol{t}$ as *virtual subcarriers*.

In our VSB model, the time-domain symbols $\boldsymbol{s}$ are real valued, so that the virtual subcarriers exhibit conjugate symmetry, i.e.,

$$t_n \;=\; \begin{cases} t_n^*, & n \in \{0, \frac{N}{2}\} \\ t_{N-n}^*, & n \in \{1, 2, \ldots, \frac{N}{2} - 1\} \end{cases}. \tag{6}$$

Using this fact, (5) can be rewritten with $\underline{\boldsymbol{t}} \in \mathbb{C}^{N/2}$:

$$\underline{\boldsymbol{x}} \;=\; \boldsymbol{\mathcal{H}}\underline{\boldsymbol{t}} + \underline{\boldsymbol{w}}, \tag{7}$$

$$\underline{t}_n \;:=\; \begin{cases} t_0 + j t_{\frac{N}{2}} & n = 0 \\ t_n & n \in \{1, \ldots, \frac{N}{2} - 1\} \end{cases} \tag{8}$$

$$\boldsymbol{\mathcal{H}} \;=\; \begin{bmatrix} A g_{\frac{N}{2}} g_0 & 0 & \cdots & 0 \\ 0 & g_1 & \cdots & 0 \\ \vdots & 0 & \ddots & 0 \\ 0 & \cdots & 0 & g_{\frac{N}{2}-1} \\ A g_{\frac{N}{2}}^* g_0^* & 0 & \cdots & 0 \\ 0 & g_{N-1}^* & \cdots & 0 \\ \vdots & 0 & \ddots & 0 \\ 0 & \cdots & 0 & g_{\frac{N}{2}+1}^* \end{bmatrix} \tag{9}$$

$$A \;=\; \left(\sqrt{|g_0|^2 + |g_{\frac{N}{2}}|^2}\right)^{-1}, \tag{10}$$

where

$$\underline{x}_n \;:=\; \begin{cases} A(g_{\frac{N}{2}} x_0 + j g_0 x_{\frac{N}{2}}) & n = 0 \\ x_n & n \in \{1, \ldots, \frac{N}{2} - 1\} \\ A(g_{\frac{N}{2}}^* x_0^* + j g_0^* x_{\frac{N}{2}}^*) & n = \frac{N}{2} \\ x_{\frac{3N}{2}-n}^* & n \in \{\frac{N}{2} + 1, \ldots, N - 1\} \end{cases} \tag{11}$$

$$\underline{w}_n \;:=\; \begin{cases} A(g_{\frac{N}{2}} w_0 + j g_0 w_{\frac{N}{2}}) & n = 0 \\ w_n & n \in \{1, \ldots, \frac{N}{2} - 1\} \\ A(g_{\frac{N}{2}}^* w_0^* + j g_0^* w_{\frac{N}{2}}^*) & n = \frac{N}{2} \\ w_{\frac{3N}{2}-n}^* & n \in \{\frac{N}{2} + 1, \ldots, N - 1\}. \end{cases} \tag{12}$$

Note that A is chosen so that $\mathrm{E}\{\underline{\boldsymbol{w}}\underline{\boldsymbol{w}}^H\} = \sigma^2 \boldsymbol{I}_N$. Essentially, (7)

removes the redundancy inherent in the VSB system model (5). We note that, with bandlimited VSB pulse shapes, some entries in $\underline{\boldsymbol{x}}$ may contain little signal energy. To reduce complexity, these elements could be ignored when estimating $\underline{\boldsymbol{t}}$. Doing so would require only that certain rows be omitted from $\underline{\boldsymbol{x}}$, $\underline{\boldsymbol{w}}$, and $\boldsymbol{\mathcal{H}}$.

We use a linear MMSE technique to estimate the virtual subcarrier vector $\underline{\boldsymbol{t}}$. In doing so, we incorporate prior statistics on $\underline{\boldsymbol{t}}$ (i.e., mean and covariance) calculated from the MAP decoder outputs during the previous iteration. To reduce complexity, however, the elements in $\underline{\boldsymbol{t}}$ are assumed uncorrelated. In this case, the MMSE estimate of $\underline{\boldsymbol{t}} \in \mathbb{C}^{N/2}$ becomes

$$\hat{\underline{\boldsymbol{t}}} = \bar{\underline{\boldsymbol{t}}} + \boldsymbol{F}(\underline{\boldsymbol{x}} - \boldsymbol{\mathcal{H}}\bar{\underline{\boldsymbol{t}}}) \quad (13)$$

$$\boldsymbol{F} = \mathcal{D}(\boldsymbol{v}_{\underline{t}})\boldsymbol{\mathcal{H}}^H\left(\boldsymbol{\mathcal{H}}\,\mathcal{D}(\boldsymbol{v}_{\underline{t}})\boldsymbol{\mathcal{H}}^H + \sigma^2\boldsymbol{I}_N\right)^{-1}, \quad (14)$$

where $\bar{\underline{\boldsymbol{t}}} := \mathrm{E}\{\underline{\boldsymbol{t}}\}$ and $\boldsymbol{v}_{\underline{t}} := \mathrm{diag}\big(\mathrm{E}\{(\underline{\boldsymbol{t}} - \bar{\underline{\boldsymbol{t}}})(\underline{\boldsymbol{t}} - \bar{\underline{\boldsymbol{t}}})^H\}\big)$. For the first iteration, we set $\bar{\underline{\boldsymbol{t}}}(i) = \boldsymbol{0}$ and $\boldsymbol{v}_{\underline{t}}(i) = \boldsymbol{1}$. Due to the sparse structure of $\boldsymbol{\mathcal{H}}$, (13) can be computed via

$$\hat{\underline{t}}_k = \begin{cases} \dfrac{Ag^*_{\frac{N}{2}}g^*_0\underline{x}_0 + Ag_{\frac{N}{2}}g_0\underline{x}_{\frac{N}{2}} + \frac{\sigma^2}{v_{\underline{t}_0}}\bar{\underline{t}}_0}{2A^2|g_{\frac{N}{2}}g_0|^2 + \frac{\sigma^2}{v_{\underline{t}_0}}}, & k = 0 \\ \dfrac{g^*_k x_k + g_{N-k}x^*_{N-k} + \frac{\sigma^2}{v_{\underline{t}_k}}\bar{\underline{t}}_k}{|g_k|^2 + |g_{N-k}|^2 + \frac{\sigma^2}{v_{\underline{t}_k}}}, & k \neq 0 \end{cases} \quad (15)$$

(16)

where $v_{\underline{t}_k} := [\boldsymbol{v}_{\underline{t}}]_k$. ¿From $\hat{\underline{\boldsymbol{t}}}$, we reconstruct $\hat{\boldsymbol{t}}$ via (6) and (8).

3.3. Generation of MAP Inputs

The soft information that is passed to the MAP decoder is computed from the conditional probabilities $\{p(\hat{s}_n|s_n = s)\}_{s\in\mathcal{S}}$, where $\mathcal{S}$ denotes the symbol alphabet. Here we describe how these conditional probabilities are generated from the equalizer outputs, and how they are passed to the decoder.

Assuming Gaussian-distributed symbol estimation error,

$$p(\hat{s}_n|s_n = s) = \frac{1}{\sqrt{2\pi\sigma^2_{n,s}}}\exp\left(-\frac{(\hat{s}_n - u_{n,s})^2}{2\sigma^2_{n,s}}\right) \quad (17)$$

$$u_{n,s} := \mathrm{E}\{\hat{s}_n|s_n = s\} \quad (18)$$

$$\sigma^2_{n,s} := \mathrm{var}\{\hat{s}_n|s_n = s\}. \quad (19)$$

It can be shown that $u_{n,s}$ and $\sigma^2_{n,s}$ can be calculated as

$$u_{n,s} = \bar{s}_n + \frac{(s - \bar{s}_n)}{N}\sum_{k=0}^{N-1} d_k \quad (20)$$

$$\sigma^2_{n,s} = \frac{\tilde{v}_n}{N}\sum_{k=0}^{N-1} d^2_k + \frac{\sigma^2}{N}\sum_{k=0}^{N-1} b_k, \quad (21)$$

where $\bar{s}_n := \mathrm{E}\{s_n\}$, $v_{s_n} := \mathrm{var}\{s_n\}$, and

$$d_k = \begin{cases} \dfrac{2A^2|g_{\frac{N}{2}}g_0|^2}{2A^2|g_{\frac{N}{2}}g_0|^2 + \frac{\sigma^2}{v_{\underline{t}_0}}} & k \in \{0, N/2\} \\ \dfrac{|g_k|^2 + |g_{N-k}|^2}{|g_k|^2 + |g_{N-k}|^2 + \frac{\sigma^2}{v_{\underline{t}_k}}}, & k \notin \{0, N/2\} \end{cases} \quad (22)$$

$$b_k = \begin{cases} \dfrac{2A^2|g_{\frac{N}{2}}g_0|^2}{\left(2A^2|g_{\frac{N}{2}}g_0|^2 + \frac{\sigma^2}{v_{\underline{t}_0}}\right)^2} & k \in \{0, N/2\} \\ \dfrac{|g_k|^2 + |g_{N-k}|^2}{\left(|g_k|^2 + |g_{N-k}|^2 + \frac{\sigma^2}{v_{\underline{t}_k}}\right)^2}, & k \notin \{0, N/2\} \end{cases} \quad (23)$$

$$\tilde{v}_n = \frac{1}{N}\sum_{k\neq n} v_{s_k}. \quad (24)$$

With punctured trellis coding, a subset of the bits that determine each symbol are left uncoded, and this influences the way that soft information is passed to and from the MAP decoder. Let us represent $s_n \in \mathcal{S}$ via $s_n \equiv [\boldsymbol{c}_n, \boldsymbol{b}_n]$, where $\boldsymbol{c}_n \in \{0,1\}^m$ and $\boldsymbol{b}_n \in \{0,1\}^{\tilde{m}}$ are vectors of coded and uncoded bits, respectively. Since the ATSC standard does not employ interleaving, we will not assume that the bits in $\boldsymbol{c}_n$ are independent. As a result, we pass $\{p(\hat{s}_n|\boldsymbol{c}_n = \boldsymbol{c}), \forall \boldsymbol{c}\}$ to the MAP decoder, where

$$p(\hat{s}_n|\boldsymbol{c}_n = \boldsymbol{c}) = \sum_{\boldsymbol{b}} p(\hat{s}_n|\boldsymbol{c}_n = \boldsymbol{c}, \boldsymbol{b}_n = \boldsymbol{b})P(\boldsymbol{b}_n = \boldsymbol{b}|\boldsymbol{c}_n = \boldsymbol{c}) \quad (25)$$

$$= \sum_{\boldsymbol{b}} p(\hat{s}_n|\boldsymbol{c}_n = \boldsymbol{c}, \boldsymbol{b}_n = \boldsymbol{b})2^{-\tilde{m}} \quad (26)$$

$$= 2^{-\tilde{m}}\sum_{s\in\mathcal{S}(\boldsymbol{c})} p(\hat{s}_n|s_n = s), \quad (27)$$

and where $\mathcal{S}(\boldsymbol{c})$ denotes the subset of $\mathcal{S}$ corresponding to bits $\boldsymbol{c}$.

3.4. Update of Virtual Subcarrier Statistics

MAP decoding yields the posterior probabilities $\{P(\boldsymbol{c}_n = \boldsymbol{c}|\hat{\boldsymbol{s}}), \forall \boldsymbol{c}\}$, which can be combined with information on the uncoded bits to update the symbol means and variances for use in the next turbo iteration. With the correspondence $s \equiv [\boldsymbol{c}, \boldsymbol{b}]$, we have

$$P(s|\hat{\boldsymbol{s}}) = P(\boldsymbol{b}|\boldsymbol{c}, \hat{\boldsymbol{s}})P(\boldsymbol{c}|\hat{\boldsymbol{s}}) \quad (28)$$

$$= \frac{p(\hat{\boldsymbol{s}}|\boldsymbol{b}, \boldsymbol{c})P(\boldsymbol{b}|\boldsymbol{c})}{p(\hat{\boldsymbol{s}}|\boldsymbol{c})}P(\boldsymbol{c}|\hat{\boldsymbol{s}}) \quad (29)$$

$$= \frac{p(\hat{\boldsymbol{s}}|\boldsymbol{b}, \boldsymbol{c})P(\boldsymbol{b}|\boldsymbol{c})}{\sum_{\boldsymbol{b}'} p(\hat{\boldsymbol{s}}|\boldsymbol{b}', \boldsymbol{c})P(\boldsymbol{b}'|\boldsymbol{c})}P(\boldsymbol{c}|\hat{\boldsymbol{s}}) \quad (30)$$

$$= \frac{p(\hat{\boldsymbol{s}}|s)}{\sum_{s'\in\mathcal{S}(\boldsymbol{c})} p(\hat{\boldsymbol{s}}|s')}P(\boldsymbol{c}|\hat{\boldsymbol{s}}), \quad (31)$$

where we used the shorthand $P(\boldsymbol{b}|\boldsymbol{c}, \hat{\boldsymbol{s}}) = P(\boldsymbol{b}_n = \boldsymbol{b}|\boldsymbol{c}_n = \boldsymbol{c}, \hat{\boldsymbol{s}})$. For (31), we assumed that $P(\boldsymbol{b}_n = \boldsymbol{b}|\boldsymbol{c}_n = \boldsymbol{c})$ is uniform over $\boldsymbol{b}$.

The posteriors $\{P(s_n = s|\hat{\boldsymbol{s}})\}_{s\in\mathcal{S}}$ from (31) are then used to update the mean and variance of s_n as follows.

$$\bar{s}_n := \mathrm{E}\{s_n|\hat{\boldsymbol{s}}\} = \sum_{s\in\mathcal{S}} sP(s_n = s|\hat{\boldsymbol{s}}) \quad (32)$$

$$v_{s_n} := \mathrm{var}\{s_n|\hat{\boldsymbol{s}}\} = \sum_{s\in\mathcal{S}} |s - \bar{s}_n|^2 P(s_n = s|\hat{\boldsymbol{s}}). \quad (33)$$

Assuming that $\{s_n\}$ are uncorrelated, the mean and variance of the virtual sub-carriers $\{t_n\}$ become

$$\bar{\boldsymbol{t}} := \mathrm{E}\{\boldsymbol{t}\} = \boldsymbol{W}\bar{\boldsymbol{s}} \quad (34)$$

$$\boldsymbol{v}_t := \mathrm{diag}(\mathrm{E}\{(\boldsymbol{t} - \bar{\boldsymbol{t}})(\boldsymbol{t} - \bar{\boldsymbol{t}})^H\}) \quad (35)$$

$$= \mathrm{diag}(\boldsymbol{W}\,\mathcal{D}(\boldsymbol{v}_s)\boldsymbol{W}^H), \quad (36)$$

where $\boldsymbol{W}_{k,n} = \frac{1}{\sqrt{N}} e^{-j\frac{2\pi kn}{N}}$. Since (36) implies that all the elements in $\boldsymbol{v}_t$ are identical, the variance calculation can be simplified to

$$v_{t_k} \;=\; \frac{1}{N}\sum_{n=0}^{N-1} v_{s_n}, \;\; \forall k. \tag{37}$$

3.5. Block Overlapping

Due to causal channel dispersion and lack of CP, the symbols near the end of the block contribute little energy to the observation. As a result, these symbols are prone to estimation errors. Figure 2 demonstrates this behavior by plotting symbol error rate (SER) versus symbol index within the block. Two traces are plotted, one for the first turbo iteration and one for the fifth. There we see that the end-of-block errors remain after several iterations. Though the CP restoration procedure attempts to mitigate this problem, the CP restoration procedure itself relies on end-of-block symbol estimates, and these fail to converge to reliable values.

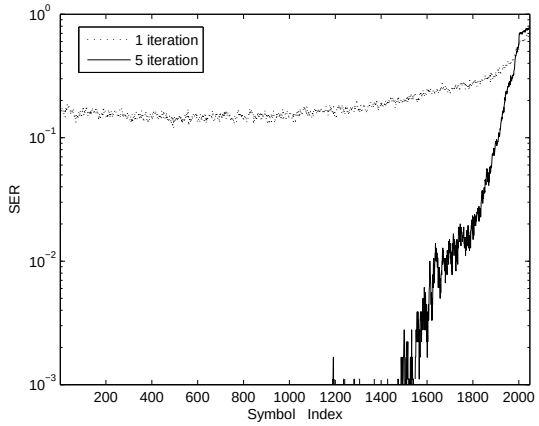

Fig. 2. Symbol error rate versus index within the block. The simulation used channel #1 from Table 1 with SNR=18dB, $N = 2048$, $L = 511$, and an average of 1000 blocks.

Because a high end-of-block SER appears to be unavoidable, we treat end-of-block symbol estimates as tentative, rather than final, estimates. To do this, we employ the block overlapping technique in Fig. 3, where only the first N_D (out of N) symbol estimates are retained as final estimates. As a result of this overlap, the overall computational complexity of FDTE scheme increases by the factor $N/(N - N_D)$. A similar block-overlap technique was applied in [15, 16].

4. NUMERICAL RESULTS

In this section, we compare the performance and complexity of the proposed FDTE with that of the DFE-plus-Viterbi-decoding (DFE-VD) method proposed by Ariyavisitakul and Li [12] with the fast DFE filter update proposed by Al-Dhahir and Cioffi [20]. In the DFE-VD scheme, the (delayed) Viterbi estimates are fed to adequately-delayed DFE feedback taps, while sub-optimal symbol-by-symbol decisions are fed to the DFE feedback taps corresponding to shorter delays.

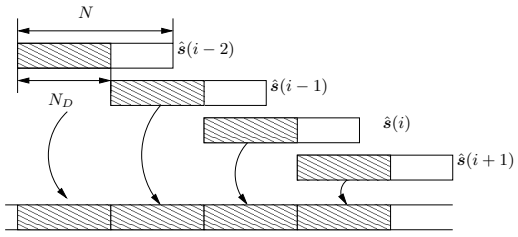

Fig. 3. The block overlapping process. Symbol estimates from the shaded part of the block are retained as final estimates.

For our performance comparison, we used the three propagation models summarized in Table 1. These were chosen similar to the ATSC R2.2 ensembles from [18]. Six paths were employed, each with a different delay, and with either a constant phase offset or a single-sided Doppler frequency spread of $f_D = 100$Hz. With the ATSC sampling rate $T_s^{-1} = 10.76$MHz, this corresponds to a normalized Doppler spread $f_D T_s = 0.00001$. The relative attenuations of the reflected paths vary among the three propagation models in Table 1; channel #1 is the least selective channel, #2 is the most time-selective, and #3 is the most frequency selective. To create the $\{h_{n,l}\}_{l=0}^{L}$, we generated propagation responses using Jakes method [19] and convolved them with the VSB pulse responses, using an overall channel order of $L = 511$.

We assumed an 8-VSB modulated single-carrier system (i.e., no CP) that used rate-$2/3$ Ungerboeck coding with constraint length 3 [17]. The receivers were assumed to have perfect channel knowledge of the channel response during the middle of each N-length block. For FDTE, we used $N = 2048$ and $N_D = N/2$, and we reconstructed a CP of length L. For DFE-VD, we updated the filter coefficients once every N_D symbols, and we used a feedforward filter of length $N_f = 2(L + 1)$ and a feedback filter of length L. The feedback filter length allows perfect post-cursor ISI cancellation, and the feedforward filter length was chosen so that further increases yielded little improvement in BER performance. The DFE-VD decoding delay was 30.

Figure 4 shows the BER performance of FDTE and DFE-VD. For these results, we averaged 200 realizations of 10 contiguous data blocks preceded by a pilot block (to prevent error propagation). From Fig. 4, we can see that, after 5 iterations, FDTE outperforms DFE-VD by 1dB (in SNR) approximately.

Table 2 specifies the cost to generate N_D symbol estimates for fast DFE-VD (with feedback filter length L) and for FDTE (per iteration). Figure 5 plots DFE-VD and FDTE complexity for the same design choices used in Fig. 4, i.e., FDTE with CP length L, $N = 4(L + 1)$, $N_D = N/2$, and 5 iterations; and DFE-VD with $N_f = 2(L + 1)$. We see that, when the channel order $L \geq 64$, the FDTE is cheaper to implement than the fast DFE-VD. Practical DTV receivers need to handle channels of order $L \approx 511$, in which case the FDTE is an order of magnitude cheaper than DFE-VD.

5. CONCLUSIONS

We presented a FDTE scheme suitable for VSB modulation with punctured trellis coding, as is used in the ATSC DTV standard. Simulations show that it outperforms the fast DFE-VD approach while maintaining up to an order-of-magnitude lower complexity.

Table 1. DTV Propagation Models.

path delay		-1.8μs	0μs	0.15μs	1.8μs	5.7μs	39.8μs
chan #1	gain	-8 dB	0 dB	-3 dB	-4 dB	-3 dB	-12 dB
	Doppler	125°	0°	80°	45°	100 Hz	90°
chan #2	gain	-8 dB	0 dB	-3 dB	-4 dB	-3 dB	-12 dB
	Doppler	100 Hz	0°	100 Hz	100 Hz	100 Hz	100 Hz
chan #3	gain	-3 dB	0 dB	-1 dB	-1 dB	-3 dB	-9 dB
	Doppler	125°	0°	80°	45°	100 Hz	90°

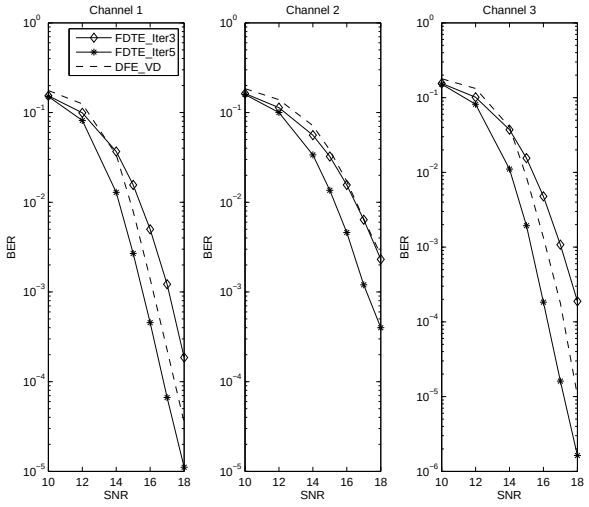

Fig. 4. BER performance for different test channels.

Table 2. Computational Complexity (per N_D symbols).

algorithm	real $\times$	real $\div$	exp	log
FDTE	$54.5N + 6N\log(N) + 11$	$6.5N + 3$	$12N$	$4N$
DFE-VT	$14N_fL + 30.5N_f + 0.5N_f^2$ $+2N_f + 2N_fN_D + LN_D$ $+8N_D - L^2 - 12L - 21$	$2N_f + N_D$	0	0

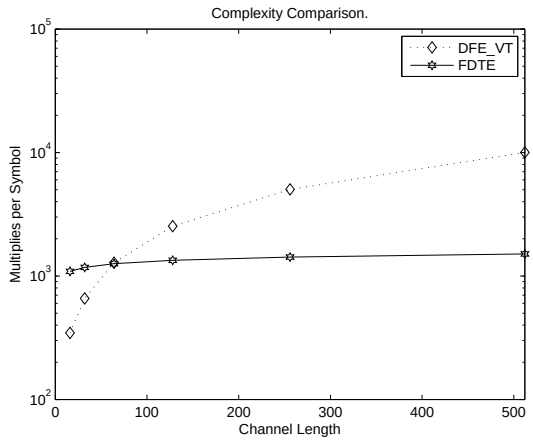

Fig. 5. Computational complexity (per symbol).

6. REFERENCES

[1] "ATSC Digital Television Standard, Rev. D with Amendment 1," from *http://www.atsc.org/standards/a_53d.pdf*, July 2005.

[2] T. Laud, M. Aitken, W. Bretl, K.Y. Kwak, "Performance of 5th generation 8-VSB receivers," *IEEE Transactions on Consumer Electronics*, vol. 50, no. 4, pp. 1076-1080, Nov. 2004.

[3] R. Behara, A. Bhaskaran, R. A. Casas, M. Gittings, M. Hryszko, S. N. Hulyalkar, and A. Touzni,"An integrated VSB/QAM/NTSC/BTSC receiver: recent advances in television design," *Proceedings of IEEE Broadcasting Symposium*, Washington, D.C., Oct. 2003.

[4] M. Ghosh "Blind decision feedback equalization for terrestrial television receivers," *Proceedings of the IEEE*, vol. 86, no. 10, pp. 2070-2081, Oct. 1998

[5] J.G.N. Henderson, W.E. Bretl, M.S. Deiss, A. Goldberg, B. Markwalter, M. Muterspaugh, and A. Touzni, "ATSC DTV Receiver Implementation," *Proceedings of the IEEE*, vol. 94, no. 1, pp. 119-147, Jan. 2006.

[6] Y. Wu, X. Wang, R. Citta, B. Ledoux, S. Lafleche, and B. Caron, "An ATSC DTV receiver with improved robustness to multipath and distributed transmission environments," *IEEE Trans. on Broadcasting*, vol 50, no. 1, pp. 32-41, March 2004.

[7] C. Douillard and M. Jezequel and C. Berrou and A. Picart and P. Didier and A. Glavieux, "Iterative correction of intersymbol interference: Turbo equalization," *European Trans. on Telecommunications*, vol. 6, pp. 507-511, Sept.-Oct. 1995.

[8] R. Koetter, A.C. Singer, and M. Tüchler, "Turbo Equalization," *IEEE Signal Processing Mag.*, vol. 21, no. 1, pp. 67-80, Jan. 2004.

[9] D. Falconer, S. L. Ariyavisitakul, A. Benyamin-Seeyar, and B. Edison, "Frequency domain equalization for single-carrier broadband wireless systems," *IEEE Commun. Mag.*, vol. 40, pp. 58-66, Apr. 2002.

[10] T. Hwang and Y. Li, "Iterative cyclic prefix reconstruction for coded single-carrier systems with frequency-domain equalization," *Proc. of Vehicular Tech. Conf.* , pp. 1841-1845, Apr. 2003.

[11] D. Kim and G. Stüber, "Residual ISI cancellation for OFDM with application to HDTV broadcasting," *Journal Select. Areas in Commun.*, vol. 16, no. 8, pp. 1590-1599.

[12] S. L. Ariyavisitakul, and Y. Li, "Joint coding and decision feedback equalization for broadband wireless channels," *IEEE Jour. Selected Areas in Communs.*, vol. 16, no. 9, pp. 1670-1678, Dec. 1998.

[13] C. Park, and G. Im, "Efficient cyclic prefix reconstruction for coded OFDM systems," *IEEE Comm. Letters*, vol. 8, no. 5, pp. 274-276, May. 2004.

[14] A. Shah, S. Biracree, R. A. Casas, T. J. Endres, S. Hulyalkar, T. A. Schaffer, and C. H. Strolle, "Global convergence of a single-axis constant modulus algorithm," *Proceedings of the Statistical Signal and Array Processing Workshop*, Pocono Manor, PA, August 2000

[15] P. Schniter and H. Liu, "Iterative Frequency-Domain Equalization for Single-Carrier Systems in Doubly-Dispersive Channels," *Proc. of Asilomar Conf. on Signals, Systems, and Computers*, pp. 667-671, Nov. 2004, Pacific Grove, CA.

[16] C.V. Sinn, J. Götze, and M. Weckerle, "Transmitter and receiver processing in block transmission systems with and without guard periods," *IEEE Proceedings in Signal Processing Advances in Wireless Communications*, Lisboa, Portual, July, 2004.

[17] G. Ungerboeck, "Channel coding with multilevel/phase signals," *IEEE Trans. Info. Theory*, vol. 28, no. 1, pp. 55-67, Jan. 1982.

[18] "ATSC Recommended Practice: Receiver Performance Guidelines," ATSC Standard A/74, from *hhtp://www.atsc.org/standards/practices/a_74_rfs.pdf*, June 2004.

[19] W. C. Jakes, *Microwave Mobile Communication*, Wiley, 1974.

[20] N. Al-Dhahir and J. M. Cioffi, "Fast computation of channel-estimate based equalizers in packet data transmission," *IEEE Trans. Signal Processing*, vol. 43, no. 11, pp. 2462-2473, Nov. 1995.